Design of a Fixed-Wing UAV Platform for Safety-Critical Autonomous Navigation Research

Karefyllis Alexandrou
Department of Mechanical Engineering
Hellenic Mediterranean University
Heraklion, Greece
tm6913@edu.hmu.gr

Alina Eqtami
Department of Mechanical Engineering
Hellenic Mediterranean University
Heraklion, Greece
eqtami@hmu.gr

***Abstract*—This paper presents the design of a fixed-wing UAV platform intended for future research in autonomous navigation, obstacle avoidance, and safety-critical control. The contribution is centered on the platform itself: a moderate-aspect-ratio low-Reynolds-number wing, a lightweight modular airframe based on 3D-printed components and carbon-fiber reinforcement, and a fuselage sized for future sensing, avionics, and onboard computation. Preliminary aerodynamic analysis is carried out in XFLR5 using Lifting Line Theory, and first-order structural estimates are used to justify the selected reinforcement strategy. The resulting platform is positioned as a practical fixed-wing research vehicle for later studies in model-based control and safety-critical navigation.**

I. Platform Concept – Aerial Robotics Testbed

The proposed fixed-wing UAV is intended to serve as an aerial robotics testbed for research in autonomous navigation, obstacle avoidance, and safety-critical control. Rather than focusing solely on flight capability, the objective is to establish a platform suitable for systematic investigation of trajectory tracking, obstacle avoidance, and safety-aware autonomous operation. For this reason, the design is driven not only by flight performance, but also by the expected requirements of onboard sensing, embedded processing, and controller implementation.

The vehicle is treated as a modular system-level platform that can accommodate future avionics, sensors, and onboard computing hardware. This approach allows the aircraft to evolve beyond an initial aerodynamic and structural prototype into a broader framework for fixed-wing aerial robotics [8]–[11]. In particular, the platform is intended to support later experimental studies on safety-critical control methodologies, including Control Barrier Functions (CBFs), in combination with trajectory-tracking and path-following controllers [6], [13], [14]. This positioning is also consistent with recent fixed-wing UAV development studies that emphasize rapid prototyping, modular integration, and mission-driven iteration as key enablers for experimental research platforms [15], [16].

From this perspective, the platform connects conceptual aircraft design with experimental autonomous-flight research, supporting future work in state estimation, trajectory planning, and real-time safe control. Compared with multirotor research platforms, a fixed-wing vehicle introduces stronger aerodynamic and maneuvering constraints, but it also offers a more relevant framework for studying endurance-oriented navigation, terrain-aware flight, and safety filtering under nonholonomic motion and flight-envelope limitations [1], [12].

*Corresponding author.

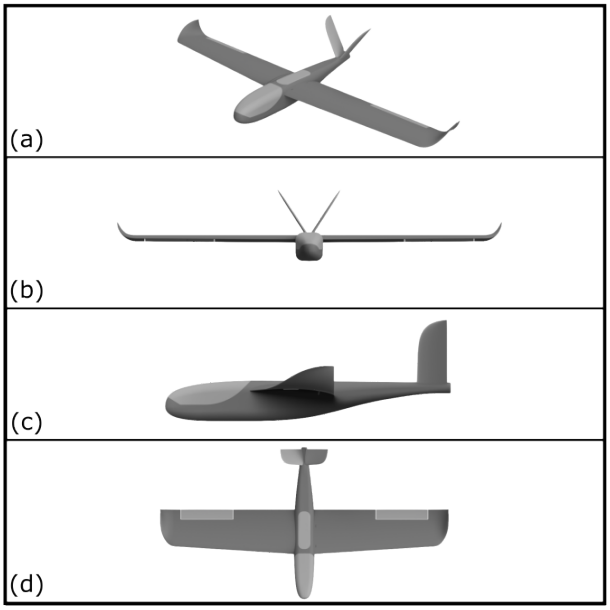

Fig. 1. Conceptual CAD views of the proposed fixed-wing UAV platform: (a) isometric view, (b) front view, (c) side view, and (d) top view. The figure illustrates the overall airframe geometry, including the wing planform, fuselage layout, and V-tail configuration.

This paper focuses on the aerodynamic and structural design of the platform. Section II presents the selected wing geometry, airfoil choice, and preliminary aerodynamic analysis carried out in XFLR5 using a Lifting Line Theory (LLT) formulation. Section III summarizes the lightweight structural concept and a first-order structural estimate of the wing-fuselage connection region. Section IV outlines the intended future control architecture that motivates the platform design.

II. Aerodynamic Design and Analysis

The wing was designed for stable, predictable performance, adequate efficiency, and ease of manufacturing, while remaining suitable for modeling and autonomous control studies.

TABLE I
PRELIMINARY WING GEOMETRY OF THE PROPOSED UAV

Parameter	Value
Wingspan	1.85 m
Root chord	0.30 m
Tip chord	0.25 m
Taper ratio	0.83
Leading-edge sweep	3.7°
Trailing-edge sweep	0°
Dihedral	1°
Mid-span twist	-1.5°
Tip twist	-3°
Wing area	0.509 m^2
Aspect ratio	6.73
Approximate MAC	0.276 m
Airfoil	SD7037

A. Wing Geometry and Design Characteristics

The selected wing has a wingspan of 1.85 m, a root chord of 0.30 m, and a tip chord of 0.25 m, giving a taper ratio of approximately 0.83. This mild taper was selected to avoid aggressive tip loading while preserving a simple and manufacturable geometry. The leading edge includes a backward sweep of approximately 3.7°, while the trailing edge remains straight.

The resulting wing area is approximately 0.509 m^2, with an aspect ratio of approximately 6.73. These values place the wing in a moderate-aspect-ratio range suitable for balancing aerodynamic efficiency, structural stiffness, and manageable flight behavior. The target all-up mass of the vehicle is approximately 3 kg, including the airframe, avionics, actuators, and a payload allowance of 0.5 kg for additional sensors or a larger battery. The design cruise speed is approximately 50 km/h (13.9 m/s), corresponding to a Reynolds number on the order of 2.6×10^5 based on the mean aerodynamic chord (MAC).

Additional spanwise shaping was introduced to improve handling and stall behavior. A dihedral angle of 1° was selected to provide passive lateral stability, while larger dihedral angles were avoided in order to preserve roll responsiveness. Washout was also incorporated, with approximately -1.5° at an intermediate span section and -3° at the wingtip. This was done to reduce the likelihood of abrupt tip stall and to help preserve aileron effectiveness near the stall boundary.

Table I summarizes the main geometric characteristics of the selected wing.

These geometric choices intentionally avoid an aggressively optimized wing in favor of a configuration with broader practical utility. For a platform expected to support future autonomous-flight experiments, moderate aspect ratio, limited dihedral, and controlled washout are more valuable when they provide repeatable flight behavior and manageable stall characteristics than when they maximize performance at a single design point.

B. Airfoil Selection

The SD7037 airfoil was selected due to its suitability for low-Reynolds-number operation in small UAVs. It offers adequate lift generation, relatively smooth aerodynamic behavior, and has already been used successfully in small aircraft and UAV-scale applications [4], [5].

The airfoil selection was based not only on aerodynamic efficiency, but also on predictable low-speed behavior and compatibility with the chosen wing configuration. This choice is consistent with the nominal cruise Reynolds number of approximately 2.6×10^5, within the low-Reynolds-number range for which the SD7037 airfoil is commonly used.

For the present platform, this low-Re compatibility is important not only aerodynamically but also operationally. At the selected moderate cruise speed, the airfoil supports meaningful lift generation without forcing the vehicle into aggressive trim conditions, which is beneficial for a stable research aircraft expected to carry avionics and future sensing payloads. In this sense, the SD7037 is consistent with the broader design objective of moderate-speed, payload-capable, and predictable fixed-wing flight rather than aggressive optimization around a narrow operating point [15].

C. Aerodynamic Modeling and Performance Estimates

At the conceptual-design stage, the aerodynamic behavior of the wing can be related to the standard lift and drag expressions

$$L = \frac{1}{2}\rho V^2 S C_L, \qquad D = \frac{1}{2}\rho V^2 S C_D \tag{1}$$

where ρ is the air density, V is the flight speed, S is the wing area, and C_L and C_D are the lift and drag coefficients, respectively. The drag behavior can also be approximated using the classical drag polar

$$C_D = C_{D0} + \frac{C_L^2}{\pi e AR} \tag{2}$$

where C_{D0} is the zero-lift drag coefficient, e is the Oswald efficiency factor, and AR is the aspect ratio [1], [2].

For steady level cruise, the lift must balance the aircraft weight, and the corresponding required cruise lift coefficient is

$$C_{L,\mathrm{cruise}} = \frac{2W}{\rho V^2 S} \tag{3}$$

where $W = mg$ is the aircraft weight. Using the current design values of $m \approx 3$ kg, $V = 50$ km/h (13.9 m/s), and $S = 0.509$ m^2, the required cruise lift coefficient is approximately $C_{L,\mathrm{cruise}} \approx 0.49$. This indicates that the selected wing operates in a natural lift range for efficient moderate-speed flight. This cruise condition is also consistent with the broader design objective of a stable and capable research platform, since it provides substantial lift capability while remaining within a favorable aerodynamic operating region.

A preliminary expression for the stall speed can also be written as

$$V_s = \sqrt{\frac{2W}{\rho S C_{L,\max}}} \tag{4}$$

Using the maximum converged lift coefficient from the present XFLR5 analysis, a conservative estimate of $C_{L,\max} \approx 1.3$ may be adopted at this stage. This gives a preliminary stall speed of approximately $V_s \approx 8.5$ m/s, or about 30.7 km/h, for the

current 3 kg design assumption. Similarly, the thrust required in steady cruise can be approximated from the aerodynamic drag as

$$T_{\text{req}} \approx D \tag{5}$$

These relations verify the consistency of the selected design parameters [1], [2].

D. Aerodynamic Analysis in XFLR5

Preliminary aerodynamic analysis was performed in XFLR5 using the Lifting Line Theory (LLT) method [2], [3]. At this stage, XFLR5 was used mainly as a rapid screening tool to compare and assess the selected geometry at low computational cost. This is useful during the conceptual design phase, where span, taper, sweep, and washout may need to be adjusted several times before moving to more detailed analysis.

The aerodynamic plots presented in Figs. 2–5 correspond to the XFLR5 LLT analysis performed at the nominal cruise condition of 50 km/h (13.9 m/s).

In the LLT framework, the wing is represented through a lifting-line approximation together with sectional airfoil polar data. The local spanwise lift per unit span can be related to the circulation distribution through

$$L'(y) = \rho V_\infty \Gamma(y) \tag{6}$$

where $\Gamma(y)$ is the circulation at spanwise location y. The induced angle of attack is then linked to the downwash field, which modifies the effective local angle of attack along the span. Although simplified, this approach captures the main influence of planform geometry and spanwise loading well enough for early design decisions [2]. The analysis focused on the lift coefficient (C_L), drag coefficient (C_D), lift-to-drag ratio (C_L/C_D), and drag polar over the range of angles of attack relevant to the expected flight envelope.

The LLT-based XFLR5 analysis converged reliably over the angle-of-attack range from approximately -5° to 14.3°. For angles above this range, the solver became unconverged, indicating the onset of strong nonlinear aerodynamic behavior and reflecting the limitations of the LLT method in the near-stall and post-stall regime. Consequently, only the converged range was used for the present aerodynamic assessment.

Figure 2 depicts the lift curve. The selected configuration exhibits an approximately linear increase in lift coefficient over most of the converged range, followed by a gradual reduction in lift-curve slope at higher angles of attack. The maximum converged lift coefficient is approximately 1.3 near the upper limit of the converged range, which is consistent with the onset of nonlinear aerodynamic behavior rather than an abrupt tip-dominated stall.

Figure 3 presents the drag results. At low angles of attack, the drag remains relatively small and is mainly influenced by the viscous contribution inherited from the SD7037 polar, while induced drag becomes increasingly important as lift rises. The drag trend remains acceptable over the intended operating region and increases more rapidly at higher angles of attack, as expected.

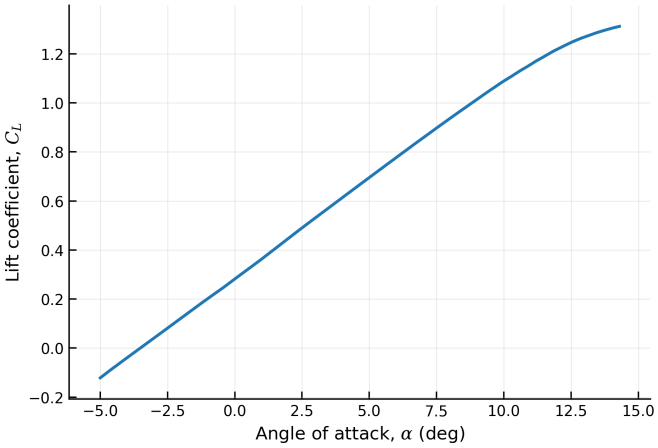

Fig. 2. Lift coefficient C_L as a function of angle of attack α for the selected wing configuration, obtained from XFLR5 LLT analysis at the nominal cruise condition.

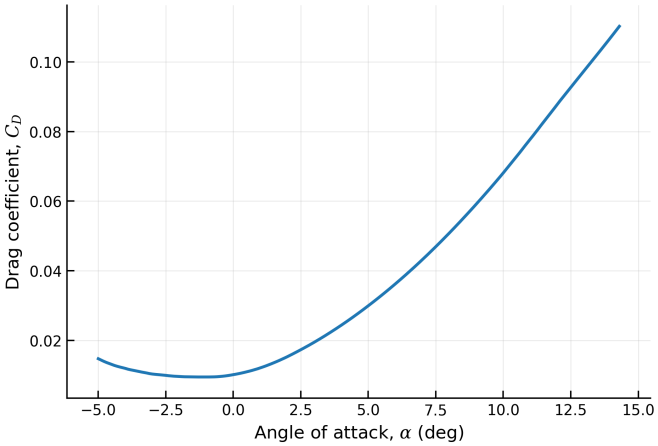

Fig. 3. Drag coefficient C_D as a function of angle of attack α for the selected wing configuration, obtained from XFLR5 LLT analysis at the nominal cruise condition.

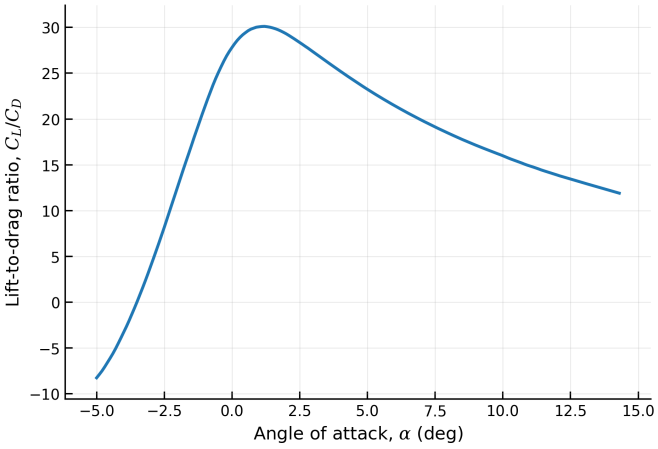

Fig. 4. Lift-to-drag ratio C_L/C_D as a function of angle of attack α for the selected wing configuration, obtained from XFLR5 LLT analysis at the nominal cruise condition.

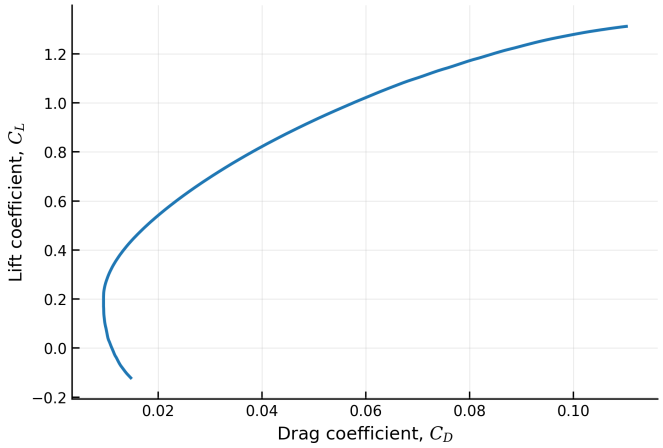

Fig. 5. Drag polar C_L versus C_D for the selected wing configuration, obtained from XFLR5 LLT analysis at the nominal cruise condition.

The lift-to-drag ratio is illustrated in Fig. 4. This plot identifies the most aerodynamically efficient operating region. The results indicate a maximum C_L/C_D of approximately 30 at a small positive angle of attack, close to $\alpha \approx 1^\circ$. This condition can be interpreted as the approximate best-efficiency cruise point of the wing. The gradual decline in efficiency at higher angles of attack is consistent with the increasing drag penalty required to generate additional lift.

The drag polar appears in Fig. 5. This curve provides a compact representation of the aerodynamic trade-off between lift generation and drag increase over the converged operating range. The smooth variation of the drag polar supports the consistency of the selected wing geometry and confirms that the configuration follows a physically reasonable aerodynamic trend within the analyzed range.

Taken together, the XFLR5 results support the selected configuration. The chosen span and chord distribution give a balanced aerodynamic response, the SD7037 airfoil behaves reasonably in the expected low-Reynolds-number range, and the combination of limited dihedral and moderate washout supports the intended handling qualities. Overall, the XFLR5 results indicate that the selected geometry provides a balanced aerodynamic response, with the airfoil and spanwise shaping supporting stable and predictable flight behavior.

From a platform-design perspective, these aerodynamic results are important not only because they indicate acceptable efficiency, but also because they suggest a wing with manageable behavior over the intended operating range. In particular, the moderate lift growth, the favorable low-angle efficiency region, and the absence of an abrupt trend change prior to the upper converged range all support the use of the vehicle as a research platform rather than a narrowly specialized aircraft. This is beneficial for later autonomous-flight studies, where repeatable trim conditions and predictable response characteristics are often more valuable than marginal gains in peak aerodynamic efficiency.

At this stage, the XFLR5 analysis serves as a preliminary design tool rather than a final aerodynamic validation. Although LLT is suitable for early comparisons, it does not capture three-dimensional effects with high fidelity. Higher-fidelity CFD will therefore be used for further refinement.

III. Structural and Platform Design

The airframe is lightweight, stiff, and modular, combining 3D-printed components with carbon-fiber reinforcement for structural integrity and integration flexibility.

A. Airframe Concept and Modularity

The airframe follows a modular design, allowing structural components to be manufactured, assembled, and replaced independently. This facilitates rapid modifications, maintenance, and integration of different payloads and subsystems.

The platform is primarily manufactured using 3D-printed ABS components. A lightweight strategy with 3–6% infill was adopted to reduce mass while maintaining structural integrity, using different infill patterns depending on local loading. Representative wing structures are shown in Fig. 6. Recent studies on rapid UAV development and additively manufactured fixed-wing structures similarly emphasize the practical value of modular and printable components for shortening design-test cycles, reducing tooling requirements, and enabling faster structural iteration [16]–[18].

A modular airframe also simplifies maintenance and repair during experimental use, since damaged sections can be reprinted or replaced without requiring a complete structural rebuild. This is especially useful for a research vehicle expected to undergo repeated configuration changes during development.

B. Carbon-Fiber Reinforcement and Structural Estimate

Carbon-fiber reinforcement was introduced at the most highly loaded structural regions. Two 10 mm carbon-fiber tubes were placed in the main fuselage–wing connection region to increase rigidity and improve the transfer of loads between the fuselage and the wing. In addition, 5 mm carbon-fiber tubes were integrated inside the wing to increase spanwise stiffness and reduce bending deformation under aerodynamic loading.

This hybrid structural approach combines the geometric flexibility of additive manufacturing with the high stiffness-to-weight ratio of carbon-fiber reinforcement, providing a lightweight structure while preserving rigidity and future design flexibility.

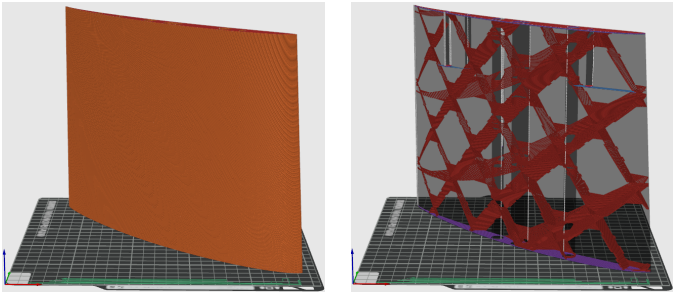

Fig. 6. Representative wing manufacturing views showing the external printed wing geometry (left) and the corresponding internal lightweight infill structure (right). The figure illustrates the low-mass printing strategy adopted for the wing while maintaining sufficient structural rigidity.

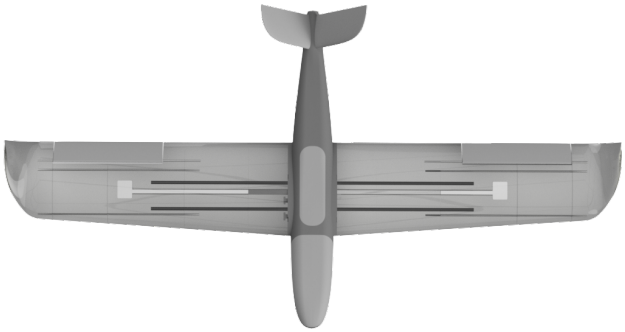

Fig. 7. Structural reinforcement layout of the proposed airframe, showing the carbon-fiber tubes integrated in the fuselage–wing connection region and within the wing for increased stiffness.

A first-order structural estimate was performed to assess the loading at the wing–fuselage connection. Assuming an approximately elliptic lift distribution, the wing root bending moment is estimated as

$$M_{\mathrm{root}} \approx \frac{nWb}{3\pi} \tag{7}$$

For the present design ($m \approx 3$ kg, $b = 1.85$ m), this results in root bending moments of approximately 5.8 N m at 1g, 17.4 N m at 3g, and 23.1 N m at 4g. The primary reinforcement consists of two carbon-fiber tubes with 10 mm outer diameter and 9 mm inner diameter, corresponding to an assumed wall thickness of 0.5 mm. Using this geometry, the section properties of each tube are approximately $I \approx 1.69 \times 10^{-10}$ m^4 and $Z \approx 3.38 \times 10^{-8}$ m^3. Assuming equal load sharing between the two main tubes, the estimated bending stresses are approximately 86 MPa at 1g, 257 MPa at 3g, and 342 MPa at 4g. These results support the selected reinforcement strategy and indicate that the structure can sustain the expected loading range at the conceptual design stage. Additional carbon-fiber tubes within the wing increase spanwise stiffness and reduce bending deformation. Higher-fidelity structural analysis will be considered in future work.

C. Manufacturing Outlook and Systems Integration

The current prototype is manufactured in ABS, while LW-ASA is considered for future iterations to reduce structural mass. Preliminary internal estimates suggest that replacing the current ABS-based bare airframe with an LW-ASA implementation could reduce the airframe mass by approximately 45%, corresponding to a reduction from about 1.8 kg to nearly 1.0 kg, depending on print settings, wall thickness, and foaming conditions.

Such a reduction in structural mass is important not only from the standpoint of flight efficiency, but also from the perspective of systems integration. A lighter empty airframe allows a larger fraction of the total mass budget to be allocated to mission-related hardware, including additional sensors, more capable onboard processing, or increased battery capacity.

The fuselage was sized not only as a structural element, but also as the main integration volume for avionics and onboard computation. In the current configuration, it accommodates the flight-control stack, power electronics, communication modules, and battery, while preserving space for future autonomy hardware such as GNSS, onboard logging, compact vision systems, range sensors, and companion computing units. In this way, the fuselage functions both as a load-bearing element and as a scalable integration space for sensing, computation, and control.

For a research platform, this systems-level modularity is as important as the airframe mass itself. The ability to reprint damaged sections, revise internal layouts, and quickly integrate new sensing or payload hardware can significantly shorten the iteration cycle between design, testing, and reconfiguration. This is one of the main practical advantages of combining additive manufacturing with a modular UAV development approach, especially when the aircraft is intended to evolve through multiple experimental stages rather than remain fixed as a single-purpose vehicle [16], [17].

Overall, the structural and platform design provides a practical basis for subsequent work in autonomous navigation, obstacle avoidance, and safety-critical flight control.

IV. Proposed Future Control Architecture

The proposed UAV platform is intended to support a control architecture combining nominal trajectory tracking with safety-critical constraint enforcement. In the present paper, this architecture is introduced to clarify the intended use of the platform rather than to report controller validation results.

At the nominal level, a model predictive control (MPC) framework is considered to generate control inputs that track a reference trajectory while respecting system dynamics and constraints. Over a finite horizon, the nominal control input can be obtained by minimizing

$$J = \sum_{k=0}^{N-1} \left[(x_k - x_k^{\mathrm{ref}})^\top Q (x_k - x_k^{\mathrm{ref}}) + u_k^\top R u_k \right] \tag{8}$$

subject to the system dynamics and admissible state and input constraints. In the present platform, these constraints represent physical and operational limitations such as bounded airspeed, altitude, roll angle, angle of attack, and actuator limits [1], [7], [12].

While MPC provides nominal trajectory tracking, safety is intended to be enforced through a Control Barrier Function (CBF) layer. Safety requirements are expressed through functions $h_i(x) \geq 0$, defining a safe operating set. For the proposed UAV, these functions correspond to conditions such as minimum separation distance from obstacles, minimum altitude, and flight-envelope limits. The final control input is then computed as the solution of the quadratic program

$$u^*(t) = \arg\min_{u \in U} \|u - u_{\mathrm{nom}}(t)\|^2 \tag{9}$$

subject to

$$\frac{d}{dt} h_i(x, u) + \gamma_i h_i(x) \geq 0, \qquad i = 1, \ldots, M \tag{10}$$

where $\gamma_i > 0$ determines the rate at which the system is driven away from unsafe regions [6], [13], [14].

In this architecture, MPC is responsible for trajectory tracking and constraint-aware control, while the CBF layer acts as a safety filter that modifies the nominal input only when necessary. This is particularly important for fixed-wing UAVs, where aerodynamic and maneuvering limitations may lead to unsafe conditions during aggressive maneuvers or in the presence of obstacles. The proposed architecture will be evaluated in future work through simulation and experimental flight testing.

V. Conclusion

This paper presented the design of a fixed-wing UAV platform intended for future research in safety-critical autonomous navigation. The contribution focused on the platform itself, including the aerodynamic design of a moderate-aspect-ratio wing based on the SD7037 airfoil, preliminary XFLR5 analysis at the nominal cruise condition, and a lightweight modular airframe reinforced with carbon-fiber structural members. The results indicate that the selected configuration provides a practical balance between lift capability, manageable aerodynamic behavior, structural feasibility, and future subsystem integration. As a result, the proposed platform provides a suitable basis for subsequent studies in fixed-wing modeling, constrained path following, obstacle avoidance, and safety-critical control. In this sense, the present work establishes both the physical platform and the initial design rationale required for subsequent fixed-wing autonomy research under realistic aerodynamic and structural constraints.

Acknowledgment

This publication is financed by the Project "Strengthening and optimizing the operation of MODY services and academic and research units of the Hellenic Mediterranean University", funded by the Public Investment Program of the Greek Ministry of Education and Religious Affairs.

References

[1] R. W. Beard and T. W. McLain, *Small Unmanned Aircraft: Theory and Practice*. Princeton, NJ, USA: Princeton University Press, 2012.

[2] J. D. Anderson, Jr., *Fundamentals of Aerodynamics*, 6th ed. New York, NY, USA: McGraw-Hill Education, 2016.

[3] A. Deperrois, "XFLR5 and Stability Analysis," XFLR5 documentation, Rev. 2.1, Nov. 2010. [Online]. Available: https://www.xflr5.tech/docs/XFLR5_and_Stability_analysis.pdf. Accessed: Mar. 14, 2026.

[4] M. Selig, "UIUC Airfoil Coordinates Database," UIUC Applied Aerodynamics Group. [Online]. Available: https://m-selig.ae.illinois.edu/ads/coord_database.html. Accessed: Mar. 14, 2026.

[5] M. S. Selig, C. A. Lyon, P. Giguere, C. P. Ninham, and J. J. Guglielmo, *Summary of Low-Speed Airfoil Data*, Vol. 2. Virginia Beach, VA, USA: SoarTech Publications, 1996.

[6] A. D. Ames, X. Xu, J. W. Grizzle, and P. Tabuada, "Control Barrier Function Based Quadratic Programs for Safety Critical Systems," *IEEE Transactions on Automatic Control*, vol. 62, no. 8, pp. 3861–3876, 2017, doi: 10.1109/TAC.2016.2638961.

[7] J. B. Rawlings, D. Q. Mayne, and M. M. Diehl, *Model Predictive Control: Theory, Computation, and Design*, 2nd ed. Madison, WI, USA: Nob Hill Publishing, 2017.

[8] S. Lupashin, M. Hehn, M. W. Mueller, A. P. Schoellig, M. Sherback, and R. D'Andrea, "A platform for aerial robotics research and demonstration: The Flying Machine Arena," *Mechatronics*, vol. 24, no. 1, pp. 41–54, 2014, doi: 10.1016/j.mechatronics.2013.11.006.

[9] P. Coen, B. Cox, O. Dantsker, and D. J. Cappelleri, "Development of a Fixed-Wing UAV Testbed for In-Flight Data Collection from an Event-Based Camera," in *AIAA SCITECH 2026 Forum*, 2026, doi: 10.2514/6.2026-2067.

[10] K. Gryte, R. Hann, M. Alam, J. Rohac, T. A. Johansen, and T. I. Fossen, "Aerodynamic Modeling of the Skywalker X8 Fixed-Wing Unmanned Aerial Vehicle," in *2018 International Conference on Unmanned Aircraft Systems (ICUAS)*, 2018, pp. 826–835, doi: 10.1109/ICUAS.2018.8453370.

[11] B. M. Witte, R. F. Singler, and S. C. C. Bailey, "Development of an Unmanned Aerial Vehicle for the Measurement of Turbulence in the Atmospheric Boundary Layer," *Atmosphere*, vol. 8, no. 10, Art. no. 195, 2017, doi: 10.3390/atmos8100195.

[12] E. M. Coates and T. I. Fossen, "Geometric Reduced-Attitude Control of Fixed-Wing UAVs," *Applied Sciences*, vol. 11, no. 7, Art. no. 3147, 2021, doi: 10.3390/app11073147.

[13] X. Lv, C. Peng, and J. Ma, "Control Barrier Function-Based Collision Avoidance Guidance Strategy for Multi-Fixed-Wing UAV Pursuit-Evasion Environment," *Drones*, vol. 8, no. 8, Art. no. 415, 2024, doi: 10.3390/drones8080415.

[14] H.-g. Kang and Y. Kim, "Control Barrier Function Based Terrain and Path Following Control of Unmanned Aerial Vehicle Considering Attitude Constraint," *Aeronautical Journal*, vol. 129, no. 1337, pp. 1960–1981, 2025, doi: 10.1017/aer.2025.22.

[15] I. Panagiotopoulos, L. Sakellariou, and A. Hatziefremidis, "Design, Construction, and Flight Performance of an Electrically Operated Fixed-Wing UAV," *Drones*, vol. 8, no. 6, Art. no. 217, 2024, doi: 10.3390/drones8060217.

[16] O. D. Dantsker, M. Theile, and M. Caccamo, "A Cyber-Physical Prototyping and Testing Framework to Enable the Rapid Development of UAVs," *Aerospace*, vol. 9, no. 5, Art. no. 270, 2022, doi: 10.3390/aerospace9050270.

[17] G. Moysiadis, S. Koltsakidis, O. Ziogas, P. Panagiotou, and D. Tzetzis, "Design and Evaluation of an Additively Manufactured UAV Fixed-Wing Using Gradient Thickness TPMS Structure and Various Shells and Infill Micro-Porosities," *Aerospace*, vol. 13, no. 1, Art. no. 50, 2026, doi: 10.3390/aerospace13010050.

[18] D. Santos, G. D. Fernandes, A. Doosttalab, and V. Maldonado, "Experimental Aerodynamics of a Small Fixed-Wing Unmanned Aerial Vehicle Coated with Bio-Inspired Microfibers Under Static and Dynamic Stall," *Aerospace*, vol. 11, no. 11, Art. no. 947, 2024, doi: 10.3390/aerospace11110947.